Aerosol and Air Quality Research, 16: 3312–3329, 2016

ISSN: 1680-8584 print / 2071-1409 online
doi: 10.4209/aaqr.2016.01.0014

Isotherm, Thermodynamic and Kinetic Studies of Selective CO_2 Adsorption on Chemically Modified Carbon Surfaces

Adedeji Adebukola Adelodun[1†], Jane Catherine Ngila[1], Do-Gun Kim[2], Young-Min Jo[3*]

[1] *Department of Applied Chemistry, University of Johannesburg, Doornfontein 2028 Johannesburg, South Africa*
[2] *Department of Health & Environmental Engineering, JEI University, Incheon, 22573, Korea*
[3] *Department of Environmental Science and Engineering, College of Engineering, Kyung Hee University, Gyenoggi-do, 446-701, Korea*

ABSTRACT

Detailed assessments of adsorption properties (isotherm, thermodynamics and kinetics) were carried out on chemically modified activated carbon (AC). Some pretreatment methods prior amination have been used to improve the CO_2 selective capture of AC in our previous works. Here, the inter-relationships among the adsorption properties were further investigated and reported. It was found that CO_2 molecules bind onto the heterogeneous surfaces of AC in a monolayer pattern as experimental data fit Freundlich isotherm rather than Langmuir. However, Redlich-Peterson, a 3-parameter model provided the best fit. The highest degree of precision of Chi-square analysis professed it as the most efficient error function for the isotherm study. Values of standard entropy showed to be the most significant thermodynamic limiting parameter in the adsorption process, as physisorption was found predominant for CO_2 collection at the interface. This observation was corroborated with temperature programmed desorption (TPD) analysis where ca. 86% of adsorbed CO_2 were desorbed below 500°C. The kinetic study indicated that CO_2-AC interaction follows pseudo-second order while the higher R^2 of intraparticle diffusion over Elovich equation confirmed the deduction made from the thermodynamic study. Conclusively, the study of adsorption properties in this work provides useful information for designing proper adsorption reactor and subsequent regeneration of CO_2-laden adsorbents at environmental levels.

Keywords: Activated carbon; Adsorption selectivity; Isotherms; Thermodynamics; Kinetics.

INTRODUCTION

There has been an increasing attention on CO_2 pollution in recent decades, in the advent of global warming. This is attributed to the accumulation of the gas from anthropogenic sources, such as the flue gas from power plants (IPCC WG, 2005; Schrag, 2007; Dantas *et al.*, 2011). In another case, CO_2 concentration is popularly used as an Indoor Air Quality (IAQ) indicator due to some health hazards (i.e., sick building syndrome (SBS)) popularly associated with exposure to its elevated levels in indoor spaces (Kulshreshtha *et al.*, 2008; Lim *et al.*, 2014). The need to lower the abnormally high CO_2 levels in both outdoor and indoor air has led to the emergence of some CO_2 capture technologies which are still under research for enhancement and optimization. Currently, the most commercialized and efficient technology for CO_2 control from point sources (such as flue gas, incineration plants, gas flaring) is absorption. The use of monoethanolamine (MEA) is very popular among the other available absorbents. However, despite the merits and popularity, absorption exhibits some inherent short-comings ((such as lack of portability, water-intensiveness and high regeneration cost (Diez *et al.*, 2015; Yu *et al.*, 2015; Gao *et al.*, 2016; Zhou *et al.*, 2016) thereby making an imperative need for a viable alternative. Among the potentially promising alternative technologies available is adsorption, especially for CO_2 capture from point sources (Xiao *et al.*, 2011; Dali *et al.*, 2012; Ma *et al.*, 2016). Of the common adsorbents available, porous activated carbons (ACs) have attracted more research attention. In comparison to MEA, AC has intrinsic advantageous features such as appreciable portability (i.e., it does not spill like solvents), readily available and low-cost precursors (any carbonaceous material), higher number of re-usability cycles, the ease of porous (morphological) and surface (chemical) modification etc. (Plaza *et al.*, 2009). Although, the conventional temperature swing adsorption

† Department of Marine Science and Technology, School of Earth and Mineral Sciences, The Federal University of Technology, P.M.B. 704, Akure, Nigeria.

* Corresponding author.
Tel.: +82 10 7121 2485; Fax: +82 31 203 4589
E-mail address: ymjo@khu.ac.kr

(TSA) used in the regeneration of AC is also energy intensive (as it ranges between 400 and 900°C), less expensive alternatives such as pressure swing adsorption (PSA), vacuum swing adsorption (VSA) and electric swing adsorption (ESA) have been optimized (Olajire, 2010; Yu *et al.*, 2012). A comprehensive cost comparison (with other sorbents) is available (as Table 4) in our recently published review work (Adelodun *et al.*, 2015). Furthermore, the CO_2 adsorption capacity by porous carbons can be greatly improved by surface modification (Shafeeyan *et al.*, 2010; Khalil *et al.*, 2012; Zhang *et al.*, 2015; Goel *et al.*, 2016). Among the available modification techniques, amination is the most popular for the impregnation of foreign nitrogen-based functionalities on activated carbon (AC) in enhancing its adsorption affinity towards CO_2 (Adelodun *et al.*, 2015).

Usually, the efficiency of an adsorbent is estimated based on its adsorption capacity, adsorption rate, mechanical strength, susceptibility to numerous regeneration cycles and reuse. Among these, adsorption capacity is considered as the most important property that is initially determined (Brdar *et al.*, 2012). It has also been suggested that when describing adsorption properties, isotherm, thermodynamic and kinetic studies are required in order to fully understand the nature, mechanism and rate of the process prior to designing the application setup (Qui *et al.*, 2009; Yousef *et al.*, 2011; Song *et al.*, 2016).

Recently, it was observed that only a few studies on the fabrication of CO_2 adsorbents have been directed to addressing selective separations from environmental levels. Instead, most researchers have focused on pure CO_2 removal capacity for their adsorption examination (Adelodun *et al.*, 2015). Due to this, our work has directly addressed CO_2 selective adsorption at the two environmental levels (indoor and flue gas), hence, it has distinct relevance to real life scenarios. Another distinction in our research work is the investigation of the significance of pre-treatment prior amination to CO_2 selective capture (Adelodun and Jo, 2013; Adelodun *et al.*, 2014a, b, 2015). The adsorption capacity (100% CO_2) as well as selectivity (10% and 0.3% CO_2) of the various modified ACs were provided in these previous works. It was gathered that the capture mechanisms and efficiencies of adsorbents toward pure and diluted levels CO_2 levels are quite dissimilar. Therefore, in current work, we furthered our research into the investigation of the mechanism (isotherm), nature/strength (thermodynamics) and rate (kinetics) of CO_2 selective adsorption on chemically modified ACs (via dry and wet pre-treatments processes prior amination).

EXPERIMENTAL

Adsorbents

Commercially available pelletized coconut shell-based and coal-based ACs, procured from Calgon Carbon Corporation (USA) were depelletized into granules (G1 and G2, respectively) and used as starting materials. Detailed information on sample preparation, structural and chemical characterizations are available in our previous works (Adelodun and Jo, 2013; Adelodun *et al.*, 2014a, b). In current work, the nomenclature and amination procedures of studied adsorbents are provided in Table 1. Their physical structures (specific surface area and porosity) were examined with the aid of Belsorp mini monosorb (Bel Japan Inc., Japan).

Assessment of CO_2 Adsorption Capacity

Pure CO_2 adsorption capacity obtained at vacuum to ambient pressure (P/P_o = 0–1) was carried out at 298 K with the aforementioned monosorb instrument while low level (0.3% in dry air) and high level (10% binary mixture with dry N2) adsorption selectivity tests were done by lab grade set-ups, equipped with SENSEair CO_2 detectors (Adelodun and Jo, 2013; Adelodun *et al.*, 2014a, b; Lim *et al.*, 2014). Schematics of these adsorption set-ups are also provided in supporting information (SI) as Figs. S1 and S2, respectively. These concentrations (0.3% and 10%) represent the mean levels of CO_2 commonly found at indoor and flue gas (emitted from coal and gas-fired plants (GCCS, 2012)) air, respectively.

Modeling of Adsorption Properties and Error Functions

Some basic reviews on various adsorption isotherm models are available in a number of literatures (Subramanyan and Das, 2009; Foo and Hamed, 2010; Yousef *et al.*, 2011; Brdar *et al.*, 2012). For current study, six appropriate models for gas-phase adsorptions were selected. These are three each of two-parameter (Langmuir (Langmuir, 1916), Freundlich (Freundlich, 1906) and Temkin (Temkin and Pyzhev, 1940))

Table 1. Detailed description test carbon samples.

Adsorbent	Pre-ozonation	Pre-calcination with KOH (under N_2 atm., 600°C, 2 h)	Amination temp.
G1			
N-G1			800°C
N-O-G1	In the presence of UV-C		800°C
1K-G1		1 M KOH	
G2			
N-G2			800°C
1K-G2		1 M KOH	
N-1K-G2		1 M KOH	600°C
N-2K-G2		2 M KOH	600°C
N-4K-G2		4 M KOH	600°C

Note. G1 and G2 are the pristine granular carbons based on coconut shell and coal, respectively.

and three-parameter (Sips (Sips, 1948), Toth (Toth, 1971) and Redlish-Peterson (Redlich and Peterson, 1959)) models, with their respective expressions provided in Eqs. (1) to (6).

$$q_e = q_{max}\frac{K_L P}{1+K_L P} \tag{1}$$

$$q_e = K_F P^{\frac{1}{n_F}} \tag{2}$$

$$q_e = B_{Te}\, lnA_{Te}\, P \tag{3}$$

$$q_e = q_{max}\frac{(K_S P)^{\beta_S}}{(1+K_S P)^{\beta_S}} \tag{4}$$

$$q_e = q_{max}\frac{K_T P}{((1+(K_T P)^{n_T})^{1/n_T}} \tag{5}$$

$$q_e = q_{max}\frac{K_R P}{1+K_R P^g} \tag{6}$$

where, q_e (mmol g^{-1}) = equilibrium adsorption capacity; q_{max} (mmol g^{-1}) = maximum adsorption capacity; K_L (L $mmol^{-1}$) = Langmuir adsorption constant; C_e = equilibrium concentration (mmol L^{-1}); K_F ((mmol g^{-1}) (L g^{-1})^n) = Freundlich isotherm constant related to adsorption capacity; n_F = Freundlich isotherm constant related to adsorption intensity; B_{Te} = Tempkin isotherm constant; A_{Te} (L g^{-1}) = Tempkin isotherm equilibrium binding constant; K_S (L $mmol^{-1}$) = Sips isotherm model constant; β_S = Sips isotherm model exponent related to surface heterogeneity; α_T (L mg^{-1}), K_T (mg g^{-1}); n_T = Toth isotherm constants; K_R = RP isotherm constant (L $mmol^{-1}$); and g = exponent in RP equation (Foo and Hamed, 2010).

Non-linear isotherm models and the adsorption kinetic modelling were carried out using Sigmaplot 10.0 software (Systat Software Inc, USA). Linear isotherm plots have become viable, easy-to-use tool for identifying and describing the best-fitting relationship in adsorption systems (Kumar, 2006; Boulinguiez *et al.*, 2008). However, due to the largely reported inherent biases resulting from the transformation accorded to the values on the abscissa and ordinate, non-linearized fittings have been suggested (Kumar, 2007; Li and Hitch, 2016). Several rigorous error functions have also been employed to determine the extent of fit distortion associated with these models (Ozacar and Sengil, 2005; Li and Hitch, 2016). However, it is important to emphasize the degree of difficulty often encountered in applying statistical softwares to linearize 3-parameter models (Foo and Hamed, 2010).

The thermodynamic parameters often considered in defining adsorption processes are the changes in standard enthalpy (ΔH^0); standard entropy (ΔS^0) and standard Gibbs' free energy (ΔG^0). These parameters can be determined from the mathematical expressions given as Eqs. (7) and (8):

$$\Delta G^0 = \Delta H^0 - T\Delta S^0 = -RT\, ln\, K_L \tag{7}$$

$$\ln K_L = -\frac{\Delta G^o}{RT} = \frac{\Delta S^o}{R} - \frac{\Delta H^o}{RT} \tag{8}$$

where, K_L = Langmuir isotherm constant, indicative on adsorption strength, and independent of qmax. The values of ΔG^o obtained from Eq. (7) at different temperatures, T are plotted against the reciprocal of T (1/T, K^{-1}) while ΔH^o and ΔS^o are extrapolated as the intercept and slope, respectively (Anirudhan and Suchithra, 2010; Yousef *et al.*, 2011).

In furtherance, the kinetics of CO_2 adsorption was also investigated using four different models viz: pseudo-first order and pseudo-second order models (chemical reaction models), intraparticle diffusion model (diffusion adsorption model) and Elovich equation (mass transfer model) (Ozacar and Sengil, 2005; Mittal *et al.*, 2007; Anirudhan and Suchithra, 2010; Yousef *et al.*, 2011; Shah and Imae, 2016; Song *et al.*, 2016). Their expressions are as given in Eqs. (9)–(12):

Pseudo-first order: $$\frac{dq}{dt} = k_1\left(q_1 - q\right) \tag{9}$$

Pseudo-second order: $$\frac{dq}{dt} = k_2\left(q_2 - q\right)^2 \tag{10}$$

Intraparticle diffusion: $$\frac{dq}{dt} = \alpha \cdot exp\left(-\beta \cdot q\right) \tag{11}$$

Elovich equation: $$R = k_{int} \cdot t^2 \tag{12}$$

where, q (mmol g^{-1}) = adsorbed CO_2 amount at time t; q_1 (mmol g^{-1}) and q_2 (mmol g^{-1}) = equilibrium adsorption amounts of pseudo first-order model and pseudo first-order model, respectively; k_1 (sec^{-1}) and k_2 (g $mmole^{-1}$ sec^{-1}) = adsorption rate constants of pseudo first-order model and pseudo first-order model, respectively. For Elovich model, α (mmole g^{-1} sec^{-1}) = constant for the initial sorption rate and β (g $mmol^{-1}$) is the constant for the parameter related to the extent of surface coverage and the activation energy of the chemisorption. In the intraparticle diffusion model, k_{int} (sec^{-1}) is the constant for the diffusion rate. All these studies on the adsorption of CO_2 were carried out and reported in this work.

RESULTS AND DISCUSSION

It is necessary to emphasize that our previous works have identified that dry phase pre-treatment of AC such as ozonation (Adelodun *et al.*, 2014a) and wet phase such as $KOH_{(aq)}$ doping (Adelodun and Jo, 2013; Adelodun *et al.*, 2014b) were most suitable for G1 and G2 respectively. This discrepancy was conclusively attributed to the difference in their degree of ultra-microporosity, as the former exhibits superiority over the latter. Furthermore, current work reports the investigation on the peculiarity of the adsorption

properties of representative samples from our previously published research works on this subject.

Textural Characteristics of Adsorbents

Comprehensive reports on the structural properties of the various amine-impregnated carbons are available in our previous works (Adelodun and Jo, 2013; Adelodun *et al.*, 2014a, b). The effects of pre-treatment and amination on the textural properties of AC could be observed by critical examination of the compiled values in Table 2. The plots of N2 adsorption isotherm at 77 K, the MP (Mikhail *et al.*, 1968) and BJH (Barrett *et al.*, 1951) for micropore and mesopore size distributions, respectively, are compared in Fig. 1(a)–1(c). It was obviously observed from Table 2 that G2 have higher S_{BET} and VT than that of G1, with the latter evincing superior microporosity. As expected, the magnitude of the SBET correlates perfectly with the amount of adsorbed N2 (Fig. 1(a)). Increasing the surface basic functionalities by amination resulted in widening of ultra-micropores (Fig. 1(b)) while the transition of supermicropores to mesopores was suspected. Upon amination, SBET and VT were somewhat enhanced, probably due to the collapse of some micropores into mesopores (Fig. 1(c)), resulting in further depreciation in value of Vmicro/VT (Table 2) (Plaza *et al.*, 2009b). Since the present amination process attempted to form the amino/nitrogen groups through chemical substitution to the surface oxides on AC pellets, surface area was not significantly decreased, differing from conventional impregnation (Shafeeyan *et al.*, 2015). In addition, the hot gas flow would significantly clear the pseudopores or cracks during the high temperature amination.

The non-stabilization of calcined KOH on AC (1K-G) resulted in more textural depreciation of G2 than G1, despite both samples exhibiting similar Vmicro. This observation is attributed to the intrinsic wider pore size characterized by G2, which allows efficient surface coating on the inner pore walls (Adelodun *et al.*, 2015; Faltynowicz *et al.*, 2015). This reduces the effect of blockage of narrower pores (supermicropores) which G1 is inherently susceptible to. Unlike simple (direct) amination, amine-stabilization of 1K-G2 (N-1K-G2) improved the carbon's Vmicro which was evident as the significant increase of Vmicro/VT from 0.805

Table 2. Compilation of textural properties of pristine and modified adsorbents.

Sample	S_{BET} (m^2 g^{-1})	V_T (cm^3 g^{-1})	dp (nm)	V_{micro} (cm^3 g^{-1})	% a_{ext}	V_{meso} (cm^3 g^{-1})	V_{micro}/V_T
G1	1143	0.505	1.77	0.432	0.90	0.074	0.855
G2	1324	0.561	1.81	0.440	0.98	0.121	0.784
N-G1	1270	0.574	1.81	0.478	1.01	0.096	0.833
N-G2	1361	0.636	1.87	0.505	1.30	0.131	0.794
N-O-G1	1291	0.611	1.85	0.483	1.06	0.128	0.791
1K-G1	1126	0.505	1.80	0.428	0.93	0.077	0.848
1K-G2	916	0.524	2.22	0.422	1.03	0.102	0.805
N-1K-G2	998	0.538	1.90	0.457	1.08	0.081	0.849
N-2K-G2	825	0.451	1.90	0.368	1.14	0.072	0.816
N-4K-G2	604	0.286	1.90	0.221	1.52	0.065	0.774

S_{BET} = specific surface area from N_2 adsorption at 77 K (using BET method); V_T = total pore volume; dp = average pore diameter; V_{micro} and V_{meso} = micropore and mesopore volume respectively; % a_{ext} = percentage external surface area; V_{micro}/V_T = proportion of micropore volume.

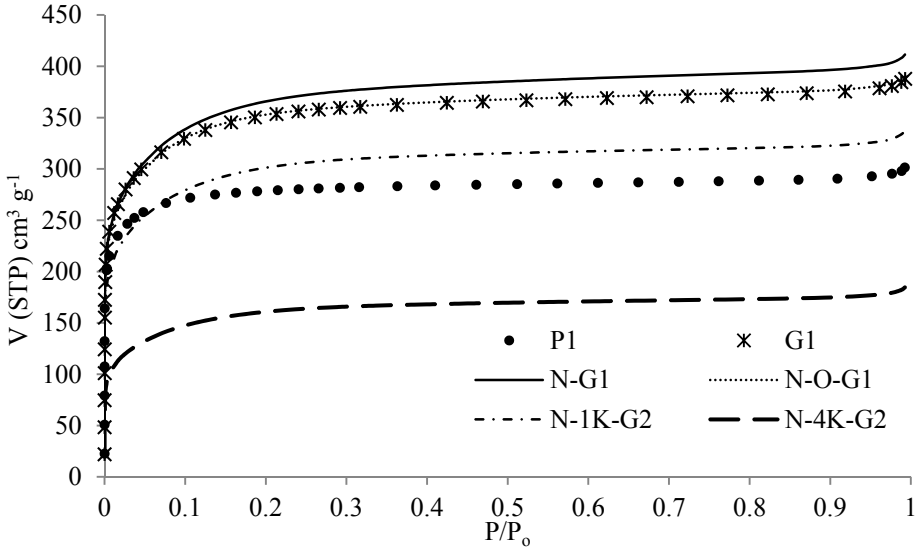

Fig. 1(a). Type I isotherm of N_2 adsorption at 77 K for selected samples.

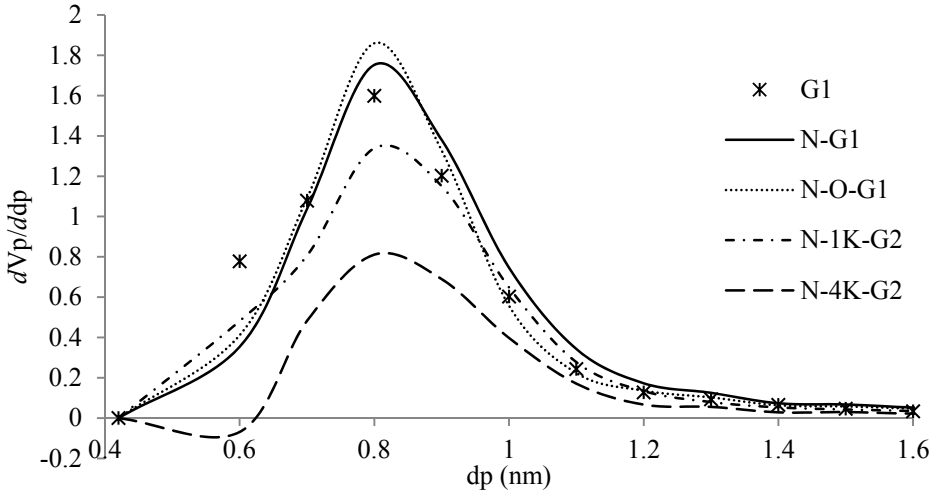

Fig. 1(b). Micropore size distribution.

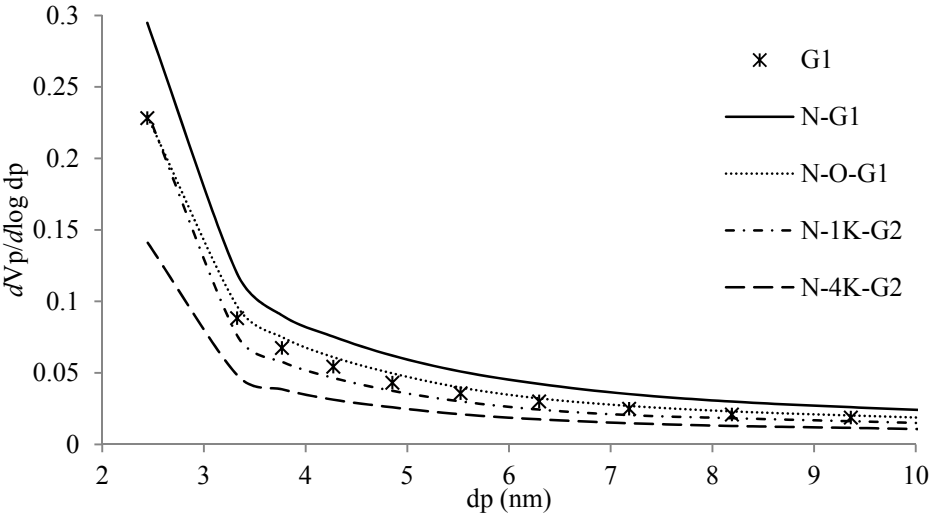

Fig. 1(c). Mesopore size distribution.

to 0.849 (1K-G2 and A-1K-G2, respectively). As expected, increase in KOH concentration led to further derogation in microporosity, which resulted from intense blockage of pores with dp ≤ 0.62 nm, evident with 4 M-doped samples, as shown in Fig. 1(b). It ensured a significant reduction (ca. 50%) in SBET, Vmicro and VT (Table 2), accompanied by significant increase in %aext, attributed to the foreign surface area provided by the potassium coating on the external layer of the graphene material (Adelodun *et al.*, 2014a, b). However, despite the lucid changes in the micropore size distribution by the different treatment conditions, all modified samples still retained the predominance of microporosity of both carbon types. This is evident by the consistent Type I isotherm portrayed by all representative samples in Fig. 1(a) (and later in Fig. 3).

CO_2 Adsorption

The CO_2 adsorption experiments were carried out in order to estimate their adsorption capacities (100% CO_2) and selective capture efficiencies for high and low levels (10% and 0.3% CO_2, respectively). Results were compared and provided in Fig. 2. It was found that amination improved the carbons' selective adsorption, which was further enhanced by dry phase pre-oxidation by ozone, especially in the presence of UV-C light (Shafeeyan *et al.*, 2011). In our review publication (Adelodun *et al.*, 2015), it was inferred that the pre-tethering of potassium active sites for the anchorage of SNFs during amine-stabilization was more efficient that those achieved with dry pre-oxidation with O3-UV (Adelodun *et al.*, 2014a, b, 2015). The chemical impregnation of basic chemical groups such as SNFs, alkali metals or their oxides on AC surface results in the decrease of pure CO_2 adsorption capacity while selective capture efficiency is enhanced (Song *et al.*, 2016). This was attributed to the fact that the capture of CO_2 from pure feed depends largely on the VT/Vmicro whilst its selective separation from a matrix is driven by the amount and nature of the basic sites with reasonably high level of affinity for the adsorbate (Shafeeyan *et al.*, 2010; Adelodun and Jo, 2013; Adelodun *et al.*, 2014a, b). For example, despite having similar textural properties in G1 and 1K-G1 (Table 3(a)), their CO_2 adsorption tendencies were quite dissimilar. Due to more developed

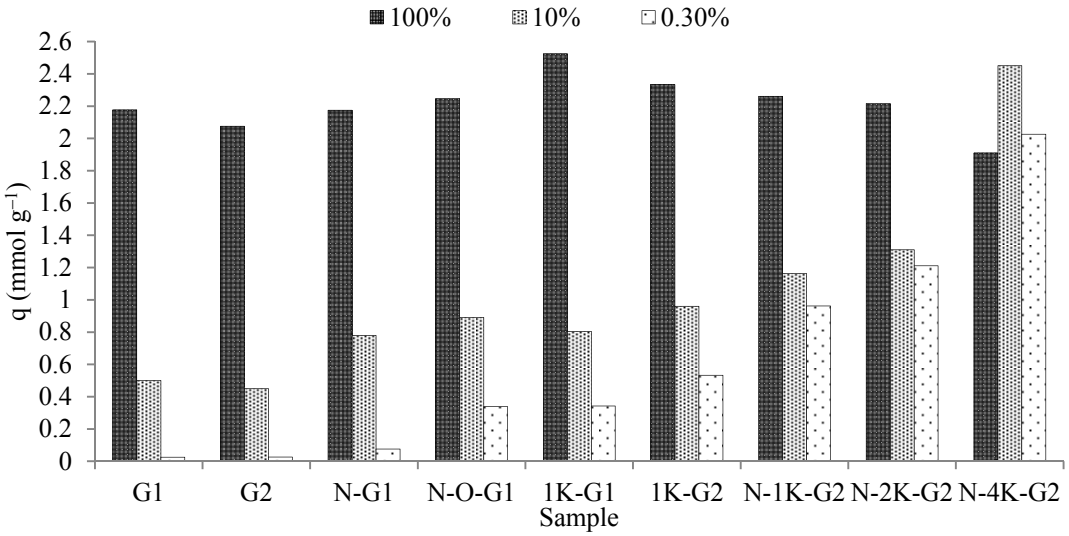

Fig. 2. CO_2 adsorption capacities of test adsorbents.

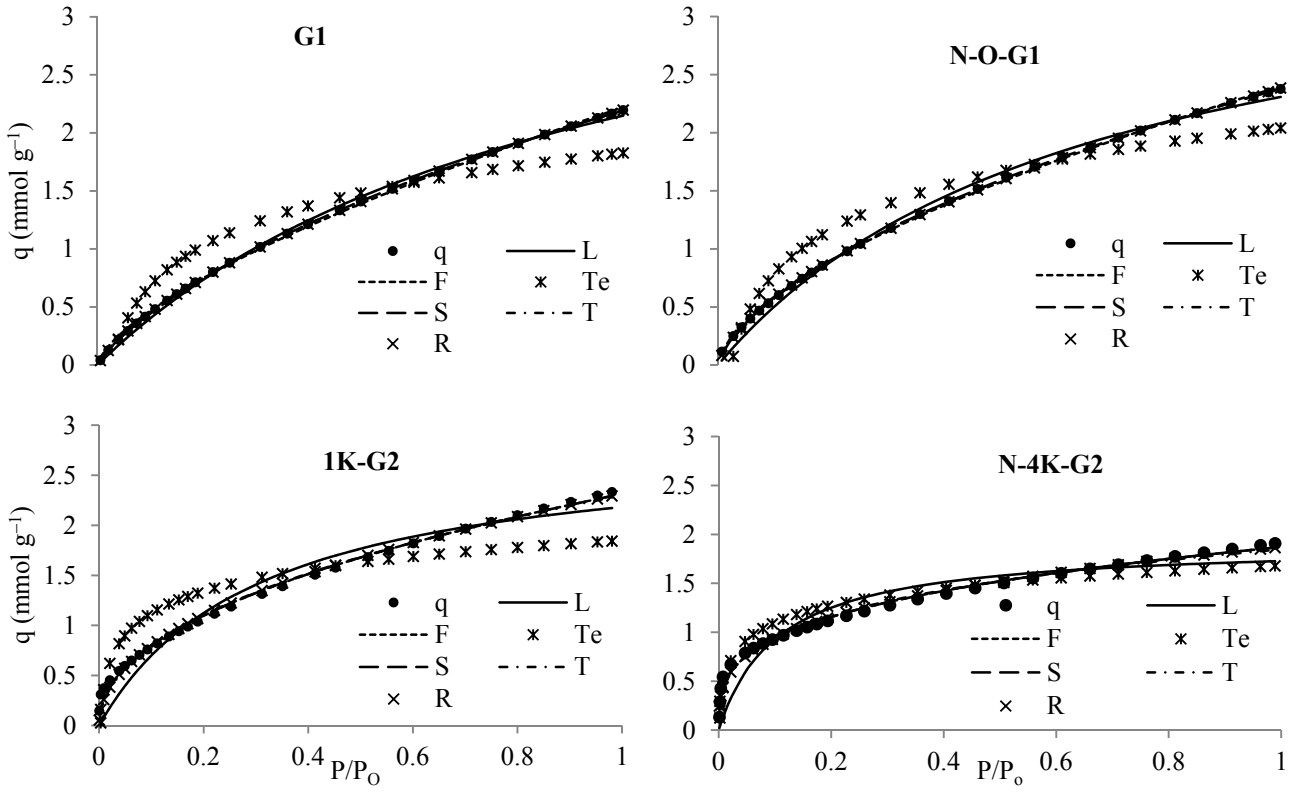

Fig. 3. Compilation of non-linear fitting of isotherm models with the experimental adsorption data.

microporosity exhibited by G1, it showed higher adsorption of pure CO_2 (Langmuir q_{max}) where competition for heterogeneous basic active sites was not required (Deng *et al.*, 2016; Kongnoo *et al.*, 2016). However, in matrices where other competitive gaseous species (such as N_2 and O_2) were present, the nature and amount of the tethered SNFs become extremely significant. This is because higher energy sites are first occupied before those of lower energies. This later scenario was described by the Sips model (Sips q_{max}) (Foo and Hamed, 2010).

Adsorption Isotherm Study and Error Functions

Fig. 3 depicts results of the statistical fitting of non-linear isotherm models to the experimental CO_2 adsorption data. The estimated adsorption parameters are compiled in Table 3(a), with the values of error estimates listed in Tables 3(b) and 3(c). By virtue of the theoretical qmax, results showed that Redlich-Peterson (R) model gave the closest values to those of experimental data (Tables 3(b) and 3(c), while all KOH-doped adsorbents exhibited the same values for both the KF of Freundlich and qmax of Redlich-

Table 3(a). Adsorption isotherm parameters of adsorption of CO_2 on test samples at room temperature.

Sample	q	Langmuir		Freundlich		Temkin		Sips			Toth			Redlich-Peterson		
	(mmol g^{-1})	q_{max}	K_L	K_F	n_F	B_{Te}	A_{Te}	q_{max}	K_S	β_S	q_{max}	K_T	n_T	q_{max}	K_R	g
G1	2.177	3.881	1.218	2.209	1.53	0.496	40.60	8.460	0.252	1.30	48.85	0.302	0.30	2.863	3.207	0.53
G2	2.076	3.933	1.083	2.124	1.47	0.457	41.96	9.877	0.183	1.30	93.87	0.141	0.26	2.772	3.130	0.49
N-G1	2.174	3.633	1.427	2.233	1.60	0.517	37.95	9.109	0.209	1.37	79.71	0.299	0.24	2.670	4.779	0.51
N-G2	2.145	3.841	1.306	2.200	1.64	0.545	42.22	10.65	0.102	1.17	116.7	0.106	0.14	2.663	8.602	0.46
N-O-G1	2.248	3.951	1.257	2.293	1.54	0.538	35.26	18.65	0.060	1.43	$1.035e^4$	0.013	0.12	2.542	8.751	0.41
1K-G1	2.525	3.598	2.056	2.545	1.81	0.427	119.0	$2.588e^4$	$5.430e^{-8}$	1.81	$2.712e^4$	0.237	0.08	2.454	$5.948e^6$	0.45
1K-G2	2.333	2.85	3.244	2.314	2.16	0.316	348.8	$7.790e^3$	$2.425e^{-8}$	2.16	$3.219e^4$	37.92	0.06	2.314	$1.781e^6$	0.54
N-1K-G2	2.261	2.741	3.483	2.248	2.23	0.324	304.3	$4.467e^3$	$4.430e^{-8}$	2.23	$7.803e^3$	76.41	0.07	2.248	$1.709e^6$	0.55
N-2K-G2	2.216	2.485	4.630	2.179	2.54	0.320	327.4	$7.616e^6$	$3.658e^{-17}$	2.51	$6.148e^3$	$3.92e^3$	0.06	2.179	$2.418e^6$	0.60
N-4K-G2	1.910	1.910	9.483	1.871	3.35	0.253	766.6	$1.632e^5$	$2.937e^{-17}$	3.35	$1.570e^2$	$8.83e^5$	0.07	1.871	$5.467e^3$	0.70

Table 3(b). Comparison of non-linear coefficient of determination and average relative error of tests samples.

Sample	Coefficient of determination (R^2)						Average relative error (ARE)					
	L	F	Te	S	T	R	L	F	Te	S	T	R
G1	0.9972	0.9991	0.8623	1.0000	1.0000	1.0000	1.0452	1.2184	15.768	0.220	0.0597	0.9373
G2	0.9973	0.9994	0.8351	1.0000	1.0000	1.0000	2.3702	1.0450	18.192	0.188	0.0430	0.0290
N-G1	0.9957	0.9992	0.8926	1.0000	1.0000	0.9999	2.5662	1.4345	14.045	0.0506	0.2437	0.3630
N-G2	0.9940	0.9996	0.8783	1.0000	1.0000	0.9998	2.9237	0.9044	14.160	0.0168	0.2103	0.3113
N-O-G1	0.9948	0.9998	0.8870	1.0000	1.0000	1.0000	2.9774	0.6808	15.163	0.0133	0.1201	0.2270
1K-G1	0.9836	0.9994	0.7974	0.9994	0.9988	0.9994	4.7331	0.2571	19.531	0.2575	0.8437	0.2575
1K-G2	0.9553	0.9995	0.7702	0.9950	0.9929	0.9950	6.8801	1.7061	20.996	1.7061	2.3362	1.7061
N-1K-G2	0.9604	0.9973	0.7782	0.9973	0.9956	0.9973	5.8592	0.6589	18.126	0.6633	1.4725	0.6589
N-2K-G2	0.9346	0.9947	0.8518	0.9947	0.9920	0.9947	2.1786	2.3205	16.493	3.0557	2.3230	2.3155
N-4K-G2	0.8868	0.9924	0.9201	0.9924	0.9891	0.9924	1.8707	1.2180	12.120	2.3255	3.5668	2.3674

Table 3(c). Comparison of non-linear sum square errors and chi-square analysis of tests samples.

Sample	Sum square errors (SSE)						Non-linear chi-square test (χ^2)					
	L	F	Te	S	T	R	L	F	Te	S	T	R
G1	0.0371	0.0207	0.2591	0.0032	0.0006	0.0017	$1.152e^{-3}$	$3.190e^{-4}$	$6.425e^{-2}$	$1.061e^{-5}$	$7.770e^{-7}$	$1.891e^{-4}$
G2	0.0341	0.0155	0.2667	0.0027	0.0011	0.0017	$1.195e^{-3}$	$2.250e^{-4}$	$8.397e^{-2}$	$7.342e^{-6}$	$3.904e^{-7}$	$1.734e^{-7}$
N-G1	0.0443	0.0188	0.2221	0.0029	0.0060	0.0078	$1.473e^{-3}$	$4.412e^{-4}$	$4.990e^{-2}$	$5.563e^{-7}$	$1.294e^{-5}$	$3.233e^{-5}$
N-G2	0.0578	0.0148	0.2585	0.0049	0.0073	0.0090	$2.093e^{-3}$	$1.930e^{-4}$	$5.552e^{-2}$	$6.730e^{-8}$	$1.051e^{-5}$	$2.300e^{-5}$
N-O-G1	0.0503	0.0091	0.2340	0.0019	0.0034	0.0044	$2.052e^{-3}$	$1.033e^{-4}$	$6.090e^{-2}$	$4.102e^{-8}$	$3.242e^{-6}$	$1.150e^{-5}$
1K-G1	0.0974	0.0179	0.3429	0.0183	0.0266	0.0183	$5.937e^{-3}$	$1.678e^{-5}$	$1.197e^{-1}$	$1.678e^{-5}$	$1.810e^{-4}$	$1.678e^{-5}$
1K-G2	0.1424	0.0476	0.3228	0.0485	0.0579	0.0484	$1.186e^{-2}$	$6.914e^{-4}$	$1.302e^{-1}$	$6.914e^{-4}$	$1.304e^{-3}$	$6.914e^{-4}$
N-1K-G2	0.1302	0.0337	0.3080	0.0343	0.0439	0.0343	$8.247e^{-3}$	$9.882e^{-5}$	$9.075e^{-2}$	$1.010e^{-4}$	$4.981e^{-4}$	$9.882e^{-5}$
N-2K-G2	0.1553	0.0444	0.2342	0.0452	0.0557	0.0452	$1.562e^{-2}$	$1.221e^{-3}$	$7.217e^{-2}$	$1.221e^{-3}$	$2.134e^{-3}$	$1.216e^{-3}$
N-4K-G2	0.1680	0.0434	0.1411	0.0442	0.0530	0.0442	$1.951e^{-2}$	$1.057e^{-3}$	$3.191e^{-2}$	$1.057e^{-3}$	$2.519e^{-3}$	$1.096e^{-3}$

Table 3(d). Summary of adsorption models with best fit, based on different error function estimations.

Adsorbent structure	R^2		ARE		SSE		χ^2	
	2-parameter	3-parameter	2-parameter	3-parameter	2-parameter	3-parameter	2-parameter	3-parameter
Raw	F	S = T = **R**	F	**R**	F	T, **R**	F	**R**
Aminated	F	**S** = T = R	F	**S**	F	**S**	F	**S**
K-doped	F = **S** = **R**		F = **S** = **R**		F	**S** = **R**	F = **S** = **R**	
Aminated K-doped	F = S = **R**		F	**R**	F	S = **R**	F	S = **R**

Peterson. The conformity became more significant as the intensity of doping was enhanced by pretreatment. Here, both Sips and Toth models also showed similar results to a reasonable extent. It was noticed that increase in %aext reduces qmax whereas improvement was made with regard to bond strength, characterized by KL, nF, ATE, βS, KT and g of Langmuir, Freundlich, Temkin, Sips, Toth and Redlich-Peterson models, respectively. Generally, as the concentration and strength of surface coating increased down the table, qmax decreases while the bond strength at the adsorption interface intensifies significantly (Foo and Hamed, 2010).

In order to accurately deduce the most suitable model for describing the adsorption process, four error functions were adopted and the results are displayed in Tables 3(b) and 3(c). Among the two-parameter models, every error estimation showed that Freundlich was the best fit for all the adsorbents. This suggests that CO_2 had undergone monolayer adsorption onto the heterogeneous surface of AC, which exhibits a non-uniform distribution of adsorption energy. It also evinced that the adsorption energy exponentially decreases as the number of available adsorption sites reduces (Freundlich 1906; Kumar, 2006). On the other hand, Temkin isotherm assumes that the adsorption energy linearly decreases as the number of adsorption sites lowers, while Langmuir isotherm assumes that the adsorption energy is uniform regardless of the number of available adsorption sites (Langmuir, 1916; Temkin and Pyzhev, 1940; Foo and Hamed, 2010). On the average, all dry-processed adsorbents (pristine, pretreated and aminated) showed excellent correlation ($R^2 > 0.999$) for the three 3-parameter isotherms. However, an exemption was noticed with adsorbents pre-treated by wet phase potassium doping, where the surfaces and pores have been intensive modified leading to greater heterogeneity.

For the sake of simplicity, deductions made from Tables 3(b) and 3(c) are summarized in Table 3(d), from which inferences were easily derived. We observed that the three-parameter models fit the mechanism of CO_2 adsorption than those of two-parameter, indicating the complexity of the adsorption process. Overall, Freundlich (F) is the most reliable two-parameter model to describe the adsorption of CO_2 on all adsorbents, while Redlich-Peterson (R) and Sips (S) fit better, courtesy of the extra parameter which improves their flexibility and robustness. Administered error functions with regard to K-doped samples showed relatively similar values for Freundlich, Sips and Redlich-Peterson (Tables 3(b) and 3(c). However, of these three, only the qmax of Redlich-Peterson showed values close to those of the qe (Table 3(a)). Hence, it is conclusive that F and R models are the most competent two- and three-parameter models, respectively, given that the extrapolated data of both models overlap considerably (Table 3 and Fig. 3). This agrees with the fact that F is a special case of R when the constant *g* is bigger than unity (1) (Foo and Hamed, 2010). Also, non-linear chi-square test is showed to be the most efficient error function for this statistically comparing the models. This confirms the observation made by Mikhail and co-researchers (Mikhail *et al.*, 1968).

For confirmatory purpose, we subjected the CO_2 adsorption data of selected samples to the popular linearized 2-parameter adsorption isotherm models in order to infer on any discrepancies with those of the original, non-linearized model forms. Although, the linearized forms have been criticized for exhibiting high level of inherent bias, due to the non-uniform derivations and transformations of the coordinates. However, they still offer confirmatory tools for the 3-parameter ones. Here, three linearized forms of Langmuir and one each of Freundlich and Temkin were experimented (Eqs (13)–(17)) (Foo and Hamed, 2010):

Langmuir 1
$$\frac{P}{q_e} = \frac{1}{K_L q_{max}} + \frac{P}{q_{max}} \tag{13}$$

Langmuir 2
$$\frac{1}{q_e} = \frac{1}{q_{max}} + \frac{1}{K_L q_{max} P}; \tag{14}$$

Langmuir 3
$$\frac{q_e}{P} = K_L q_{max} - K_L q_e; \tag{15}$$

Freundlich
$$\ln\left(q_e\right) = \ln K_F + \frac{1}{n_F} \ln P \tag{16}$$

Temkin
$$q_e = B_{Te} \ln A_{Te} + B_{Te} \ln P \tag{17}$$

Representative plots are displayed in Fig. 4 and the extrapolated values provided in Table 4. The results generally showed the best fit toward Freundlich, while a slight deviation was observed with N-4K-G2, which tend to comparatively follow Langmuir I. The results presented in Table 4 also showed an increase in R^2 of Langmuir I and Langmuir II for N-1K-G2, N-2K-G2, and N-4K-G2, indicating that the homogeneity of the adsorbents for CO_2 adsorption increased with KOH concentration (Hamdaoui and Naffrechoux, 2007). This observation is attributed to the intense surface coating at high KOH concentration, leading to homogenous distribution of the active sites, which were provided by the wet-phase impregnation. This observation confirms that the adsorption of most CO_2 molecules occurred at low level, signifying the preference of the modified adsorbents for the separation of low level CO_2. Therefore, it indicates that the modified adsorbents are particularly excellent for indoor use. Similar trend was observed with Temkin plot, which overall, indicates the increase in even distribution of highly energetic active sites as earlier mentioned. In comparison, Langmuir III showed the worst fit to CO_2 adsorption on all adsorbents (Hamdaoui and Naffrechoux, 2007; Foo and Hamed, 2010). Hence, we deduced that when a linearized form is carefully chosen (as Langmuir could be linearized in multiple ways), reliable results giving detailed understanding of the adsorption mechanism could be arrived at. Also, simpler, linearized isotherm models can efficiently substitute for the more tedious non-linearized ones (which nonetheless are more reliable) where required and suitable statistic tools are far-fetched.

Estimation of Thermodynamic Parameters

In order to investigate the strength of interaction between

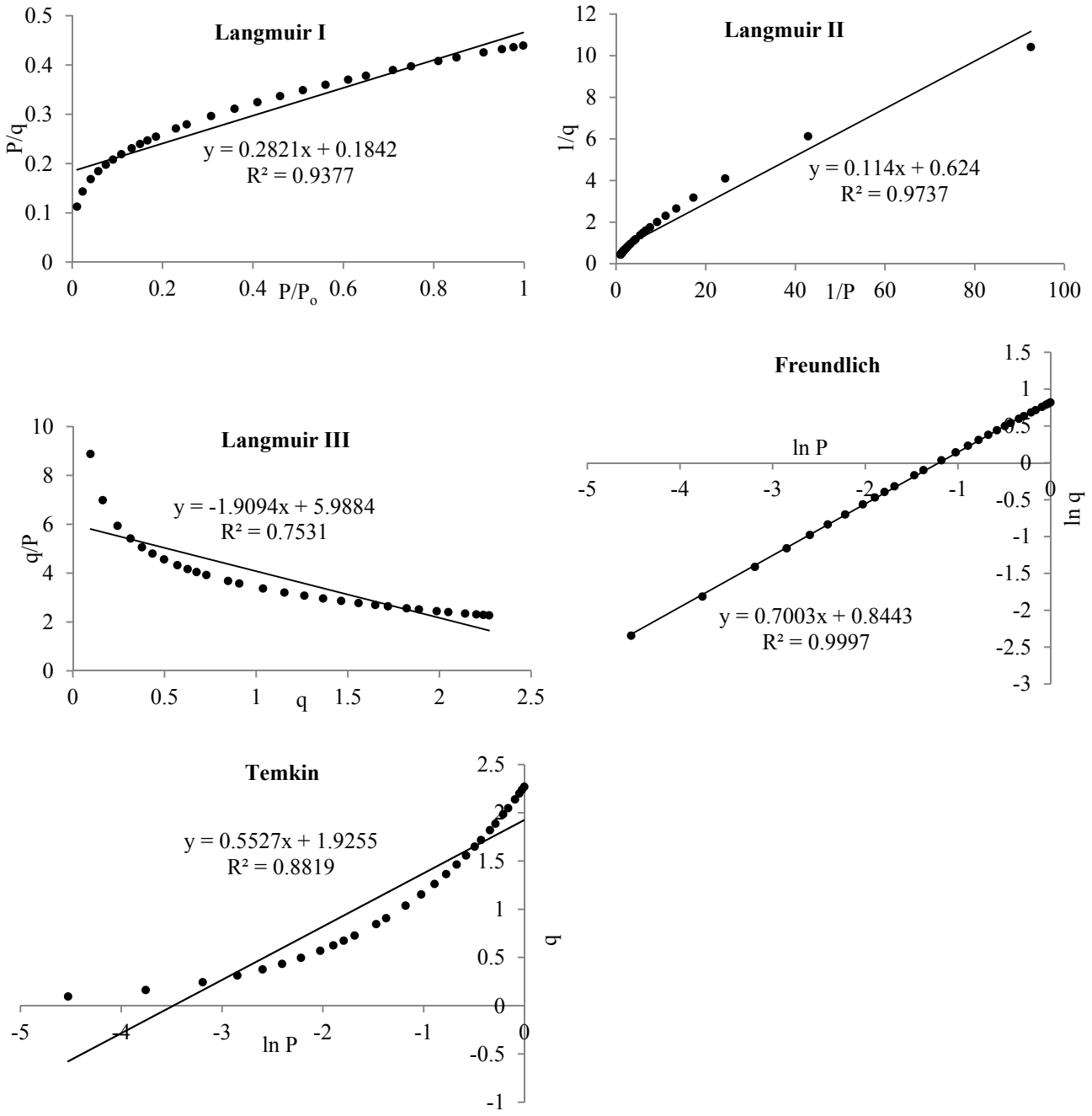

Fig. 4. Linearized plots of two-parameter models.

Table 4. Estimated isotherm parameters obtained from linearized forms.

Adsorbent	Langmuir I			Langmuir II			Langmuir III			Freundlich			Temkin		
	q_{max}	K_L	R^2	q_{max}	K_L	R^2	q_{max}	K_L	R^2	n	K_F	R^2	B_{Te}	A_{Te}	R^2
G1	3.514	1.465	0.9558	1.645	4.602	0.9955	3.183	1.736	0.8356	1.352	2.344	0.9967	2.340	39.11	0.8516
N-G1	3.545	1.531	0.9377	1.603	5.472	0.9737	3.136	1.913	0.7531	1.432	2.326	0.9997	0.553	32.41	0.8819
N-O-G1	3.116	1.965	0.9300	1.282	10.71	0.9266	2.624	2.842	0.6038	1.578	2.210	0.9993	0.511	39.15	0.8760
1K-G1	3.018	3.347	0.9238	1.050	108.2	0.7252	2.108	12.75	0.2355	2.085	2.358	0.9838	0.467	118.9	0.7740
N-1K-G1	2.467	5.237	0.9511	1.018	655	0.6582	1.698	63.79	0.1464	2.834	2.006	0.9591	0.316	322.4	0.7759
G2	3.030	1448	0.9601	1.5856	4.610	0.9910	3.323	1.684	0.9211	1.274	2.340	0.9985	2.511	36.78	0.8873
1K-G2	2.404	5.753	0.9365	0.9671	544	0.7729	1.646	59.73	0.1872	2.804	2.019	0.9715	0.297	402.1	0.7695
N-2K-G2	2.352	6.327	0.9551	1.2706	109	0.9373	1.764	32.82	0.4197	2.772	2.091	0.9831	0.313	347.6	0.8531
N-4K-G2	1.916	10.74	0.9756	1.326	103	0.9627	1.525	60.21	0.5987	3.203	1.906	0.9527	0.249	21.25	0.9226

CO_2 and AC at the sorbate-sorbent interphase, the CO_2 adsorption behavior of seven selected samples at four different temperatures (273, 288, 298, 308 K) was examined. The adsorption profile of representative two are shown in Fig. 5. As earlier indicated, two possible plots from which thermodynamic parameters could be derived ($\ln K_L$ vs. $1/T$ and ΔG vs. T) are compared as displayed as Fig. 6. We also attempted the use of Freundlich constant for adsorption strength, n_F, in lieu of customary K_L, considering the better conformity of the adsorption process with Freundlich than Langmuir. To this respect, despite the better fitness of Freundlich over Langmuir, the estimated data (from the plots of $\ln n_F$ vs. $1/T$ and ΔG (n_F) vs. T) proved such substitution to be unrealistic and hence unreliable. This could be envisaged from the near-plateau slope of the plot when n_F was used. Therefore, the obtained values were not considered in this work. However, we affirm from this examination that n_F cannot be substituted for K_L despite the aforementioned reason for such study.

In furtherance, by the virtue of the regression coefficient (R^2) provided in Table 5 along with the thermodynamic parameters, the plot of $\ln K_L$ vs. $1/T$ provides more reliable thermodynamic expression than the plot of ΔG vs. T, although the difference between their respective R^2 was not excessively high. This was evidently replicated in the proximity of the extrapolated parameters between the two plots. Hence, the plot of $\ln K_L$ vs. $1/T$ suits the thermodynamic study of CO_2 on modified ACs than the ΔG vs. T plot.

From Table 7, the negative values of ΔH^o indicate the exothermic nature of CO_2 adsorption, which progressively increases with increase in the magnitude of surface basic treatment and heterogeneity. It is suggested that the higher ΔH^o for 1K-G2 over N-1K-G2 was due to the presence of K_2O on the former, which have been replaced by surface nitrogen functionalities (SNFs) on the latter during stabilization by amination. A hypothetical model for the chemisorption of CO_2 by K-pre-doped and aminated AC surface is provided as Supporting Information (Fig. S3).

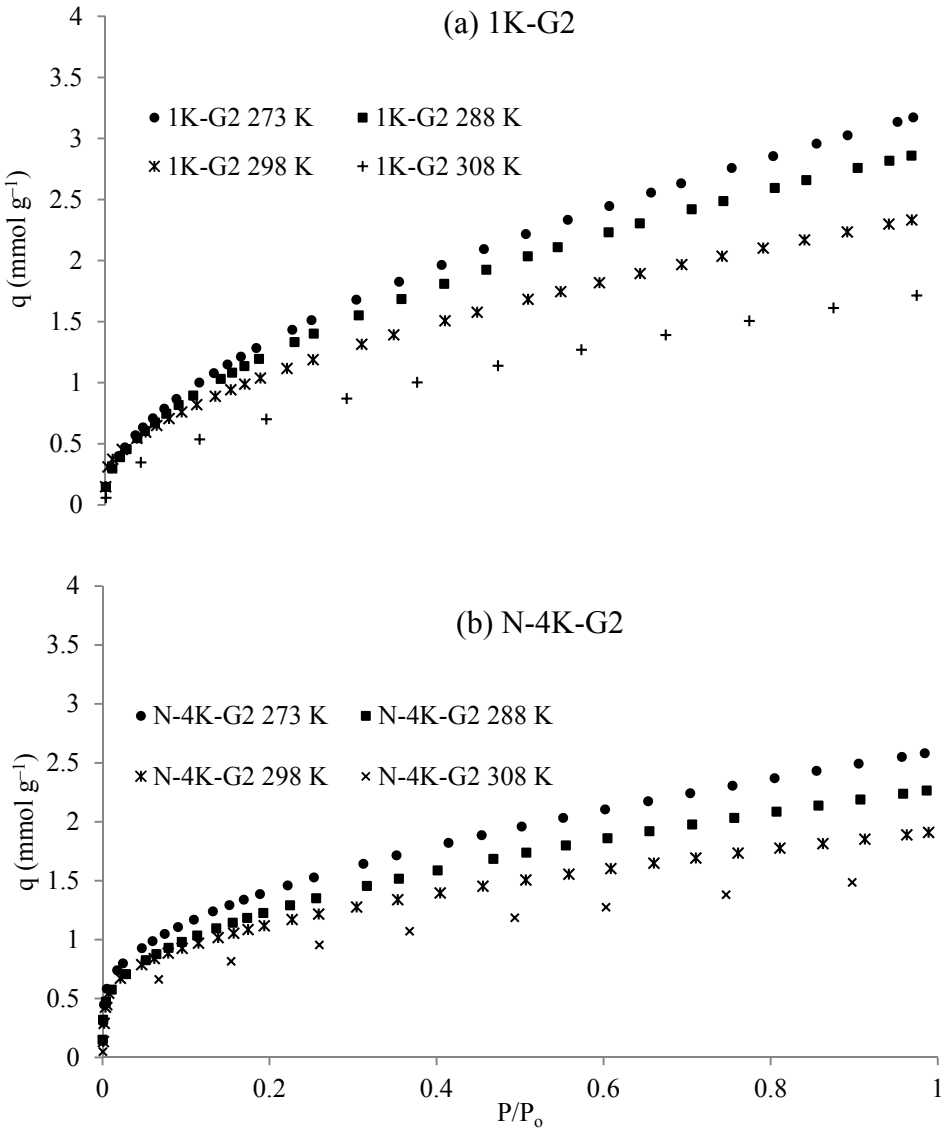

Fig. 5. Plots of CO_2 adsorption data of (a) 1K-G2 and (b) N-4K-G2 samples at different temperatures.

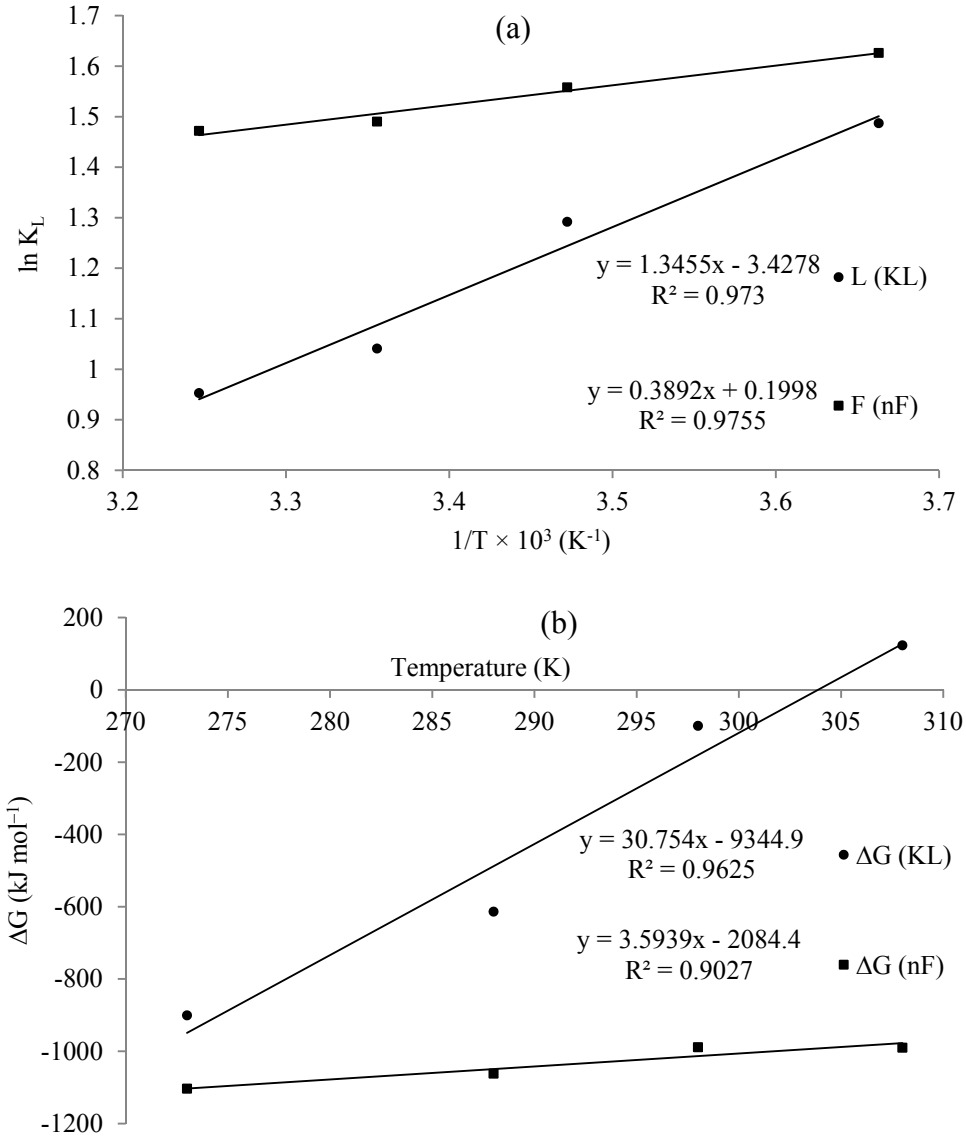

Fig. 6. A representative plot of (a) ln K_L vs. 1/T and (b) ΔG vs. T for estimating thermodynamics parameters.

Table 5. Thermodynamic data for adsorption of CO_2 on chemically modified carbons.

Adsorbent	ln K_L vs. 1/T			ΔG vs. T			Gibbs free energy, ΔG			
	ΔH^o	ΔS^o	R^2	ΔH^o	ΔS^o	R^2	273 K	288 K	298 K	308 K
G1	–9.880	–25.12	0.9841	9.032	26.84	0.9770	–3.255	–2.839	–2.308	–2.157
N-G1	–11.20	–28.50	0.9730	9.345	30.75	0.9625	–3.375	–3.094	–2.580	–2.440
N-O-G1	–12.88	–30.30	0.9838	9.410	31.28	0.9782	–3.952	–3.676	–3.237	–2.650
G2	–9.514	–24.63	0.9926	9.141	28.77	0.9695	–3.410	–3.051	–2.488	–1.990
1K-G2	–26.34	–69.65	0.9778	10.53	28.68	0.9403	–4.671	–4.232	–4.134	–3.596
N-1K-G2	–22.17	–48.31	0.9627	14.53	45.98	0.9444	–4.852	–4.747	–4.516	–3.394
N-4K-G2	–30.74	–53.11	0.8743	32.42	76.24	0.8578	–7.756	–7.551	–7.462	–7.283

The ΔH^o values of G1, N-G1 and N-O-G1 suggest that CO_2 molecules were collected on these adsorbents by physisorption (2–20 kJ mol^{-1}), while those with KOH-modified adsorbents (1K-G2, N-1K-G2, and N-4K-G2) are significantly above 20 kJ mol^{-1}, although not yet in the well-defined region of chemisorption ($\Delta H^o \geq 40$ kJ mol^{-1}) (Yousef *et al.*, 2011). From this deduction, the prevalence of physisorption over chemisorption was confirmed. The positive values of ΔS^o reflect the progression of adsorption towards equilibrium within the system. With increasing ΔH^o, ΔS^o increases, which indicates that more CO_2 molecules tend to collect at the solid surface with higher

bond strength. A higher value of ΔS^o signifies a higher degree of freedom or randomness of CO_2 molecules that were adsorbed on the modified surface than in the bulk gas phase (Erdem *et al.*, 2103).

By estimation, it was found that ΔH^o was higher than $T\Delta S^o$, which infers the dominant influence of entropy over enthalpy within the system (Foo and Hamed, 2010). This could be confirmed by the discrepancies between the ΔH^o and ΔS^o values of K-doped samples. For instance, sample 1K-G2 with no doped SNFs, is expected to show higher ΔH^o over N-IK-G2, as well as N-4K-G2, regardless of the difference in the KOH concentration difference. Only the values of ΔS^o with $\ln K_L$ vs. $1/T$ plot conform adequately with this expectation (Table 5). Again, this attests to the reliability of $\ln K_L$ vs. $1/T$ over ΔG^o vs. T. Most importantly, the negative values of ΔG^o show that the adsorption is thermodynamically favorable and spontaneous (Yousef *et al.*, 2011). In addition, the values of ΔG^o up to 20.0 kJ mol^{-1} is consistent with electrostatic interaction (physisorption) (Anirudhan and Suchithra, 2010), where adsorption by dative covalent bonding or complexation (range of 21.0 and 40.0 kJ mol^{-1}) is assumed to have taken place. Here, our results showed that attraction of CO2 by the adsorbents in this study is mainly by van Der Waal's forces, which in theory, would enable easy refreshment of the adsorbent during thermal, pressure or electric regeneration (Anirudhan and Suchithra, 2010; Yousef *et al.*, 2011).

Adsorption Kinetics Study

Theoretically, the pseudo first-order model generally provides good fit when the mass of an adsorbate on an adsorbent surface is low and the adsorption amount reaches a plateau, whereas the pseudo second-order model is suitable when the concentration of an adsorbate on an adsorbent is high, and the adsorption amount does not reach an equilibrium (Song *et al.*, 2016). In other words, the pseudo second-order model is suitable to demonstrate the dependency of adsorption rate on the sorption capacity of a surface (Aharoni and Tompkins, 1970; Ho and Ofomaja, 2006; Valderrama *et al.*, 2007; Cáceres-Jensen *et al.*, 2013). The fitting of experimental data with adsorption kinetic models are provided in Fig. 7, and the estimated kinetic parameters are presented in Table 6. The low R^2 (in Table 6 and Fig. 7(a)) clearly shows the poor fitting of pseudo-first order model whereas pseudo-second order model showed excellent fit to all experimental results, evincing the R^2 values of near unity. This opines that the CO_2 adsorption onto the surfaces of the adsorbents in this study is governed by the adsorbate amount on the surface of the adsorbents (Ozacar and Suchithra, 2010).

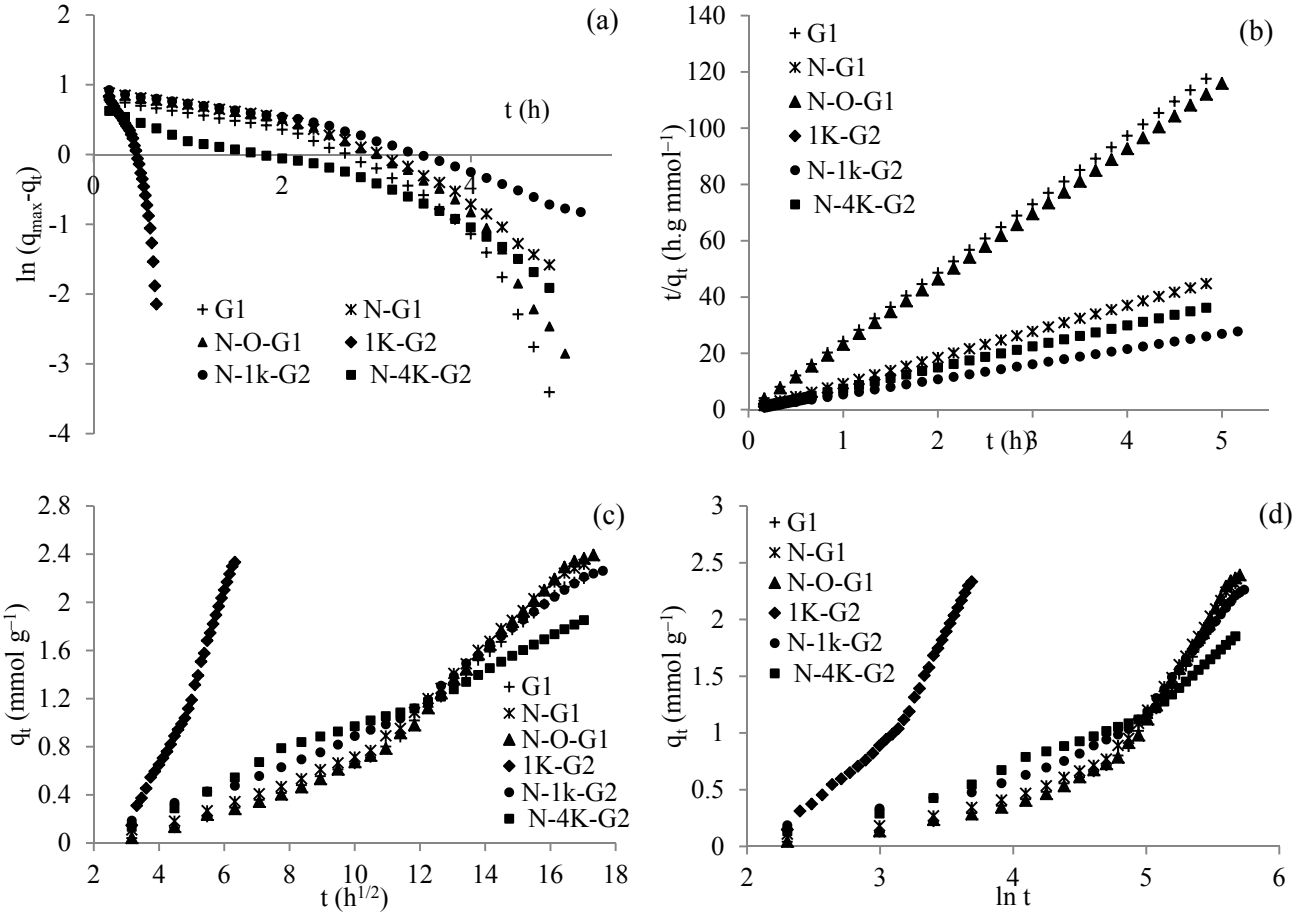

Fig. 7. 10% CO_2 adsorption fitted into (a) pseudo-first order, (b) pseudo second order, (c) intraparticle diffusion and (d) Elovich equation models.

Table 6. Kinetic parameters for adsorption of 10% CO_2 on the modified carbons at 30°C.

Adsorbent	Pseudo-first-order			Pseudo-second-order			Intraparticle diffusion		Elovich equation		
	q_1 (mmol g^{-1})	k_1 (sec^{-1}) × 10^{-5}	R^2	q_2 (mmol g^{-1})	$k_2 \times 10^{-3}$ (sec $mmol^{-1}$ sec^{-1})	R^2	$k_{int} \times 10^{-3}$ (mmol g^{-1} $sec^{-1/2}$)	R^2	α (× 10^{-4})	B (× 10^2)	R^2
G1	0.473	2	0.8609	0.483	522.6	0.9999	0.91	0.9972	5.56	25	0.8062
N-G1	0.493	0.9	0.9121	0.662	24.15	0.9999	4.06	0.9915	2.78	50	0.8860
N-O-G1	0.694	0.7	0.9371	0.860	18.77	0.9998	4.25	0.9900	2.83	2.91	0.8970
G2	0.413	2	0.9084	0.474	516.3	0.9984	0.88	0.9973	4.85	30	0.8457
1K-G2	0.893	9	0.9887	1.503	5.046	0.9838	1.42	0.9781	3.66	1.54	0.9941
N-1K-G2	0.961	5	0.9936	1.081	27.81	0.9999	0.80	0.9927	16.8	3.03	0.9922
N-4K-G2	1.45	3	0.9823	2.455	24.83	0.9981	0.71	0.9872	9.99	3.33	0.9962

In general, the CO_2 attachment on AC was found to be more of diffusion-driven than by the formation of chemical bonds as the intraparticle diffusion model provided better fits than Elovich for all the adsorbents. This hypothesis confirms the dependence of adsorption on ΔS^o over ΔH^o as found in thermodynamics study. Meanwhile, the KOH-modified adsorbents (1K-G2, N-1K-G2 and N-4K-G2), that showed high surface energies, exhibited better fits to Elovich equation, than aminated or virgin adsorbents (G1, N-G1, and N-O-G1). This indicates that the pretreatment by KOH provides the adsorbent with extra adsorption mechanisms besides diffusion. The Elovich equation describes an adsorption process as a group of reactions including diffusion of the bulk phase, surface diffusion, and active catalytic surfaces (Dabrowski, 2001). Also, Elovich considers the variation of chemisorption energetics in relation to the extent of surface coverage and the decrease in the sorption rate (Aharoni and Tompkins, 1970). The chemisorption of CO_2 at some degree has also been observed earlier for K-pre-doped samples (such as 1K-G2 and N-4K-G2) (Adelodun *et al.*, 2015). Therefore, it is suggested that CO_2 adsorption on the KOH-modified adsorbents is attributed to both chemisorption and physisorption. The peculiar sorption of CO_2 by K_2O on 1K-G2, compared to SNF on other samples was distinctly indicated by the wide digression in the kinetic plots of pseudo-first order, intraparticle diffusion and Elovich equation. With the pseudo-second order, we observed that the comparative adsorption process that reached completion in 45 min with 1K-G2 took ca. 5 h by other samples (Fig. 7(b)). These observations agree to the theory that in an adsorption system, chemisorption occurs before physisorption as adsorption sites with higher energy levels are occupied first (Ozacar and Sengil, 2005; Mittal *et al.*, 2007; Anirudhan and Suchithra, 2010).

From the study of these adsorption properties, it is believed that the nature and concentration of surface chemical functionalities is predominantly responsible for the enhanced CO_2 selectivity, despite the lowering of pure level adsorption efficiency (Fig. 2). This is clearly shown by the pure CO_2 adsorption plot of the representative samples compared in Fig. 8 (Adelodun *et al.*, 2014b). As depicted, the adsorption profiles indicate that samples with no potassium species tethered on their surfaces barely adsorbed any CO_2 molecules in the early period of the adsorption process (0–0.0005 P/Po), whereas those with higher surface energy exhibited immense adsorption at this early stage. Up to ca. 0.4 P/Po, the relevance of surface chemistry was dominant. As the partial pressure (concentration) of CO2 increases (0.5 to 1 P/Po), physical adsorption becomes the main mechanism of CO_2 collection on the adsorbent. Consequently, the findings in this work affirm the fundamental principle of adsorption that it is process more efficient for low level separation from previous works (Shafeeyan *et al.*, 2010; Adelodun *et al.*, 2015).

Thermal Programmed Desorption (TPD) Test for CO_2 Adsorption

In order to estimate the amount of CO_2 chemically adsorbed by basic species, a modified sample N-4K-G2,

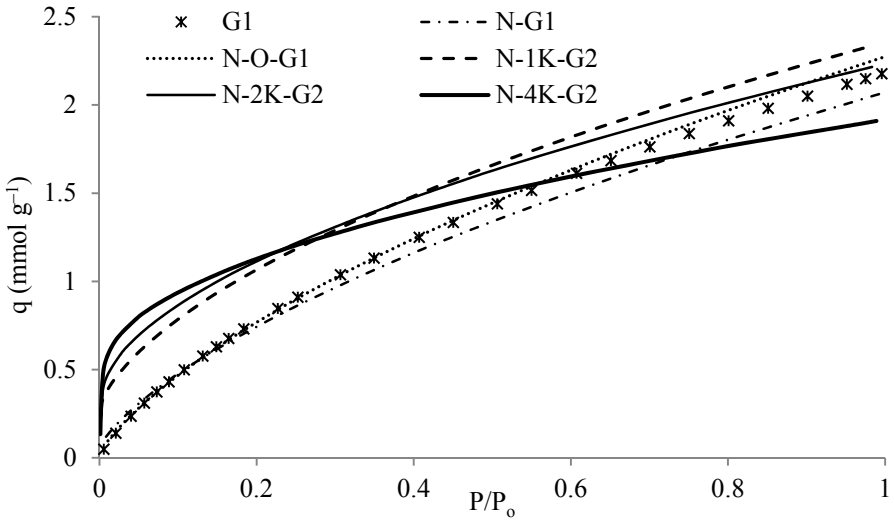

Fig. 8. Pure CO_2 adsorption profile showing significance of surface modification on selective adsorption.

which showed the best result for selective CO_2 adsorption, was subjected to TPD test. Under N_2 flow, N-4K-G2 laden with 10% CO_2 flow was ramped up to 600°C at a heating rate of ca. 20 °C min^{-1} while the quantity of desorbed CO_2 was continuously monitored (Fig. 9). The TPD profile gave a reliable segregation of desorbed CO_2 at predetermined set temperatures of 25, 100, 200, 300, 400, 500 and 600°C, which was kept for *ca.* 12 min each prior to the next so as to ensure reliable quantitation of CO_2 released at each temperature. Fig. 9 expresses a stepwise temperature programmed desorption, which was used to quantify the amount of CO_2 evolved at each temperature, intermittently. An additional continuous TPD provided in SI (Fig. S4) was carried out to validate of the reliability of CO_2 quantitation data from Fig. 9. It was revealed that most adsorbed CO_2 molecules were desorbed between room temperature and 400°C, which suggested that CO_2 interaction with the tethered SNF on AC was predominant (Yousef *et al.*, 2011). Quantification of desorbed CO_2 is reported in Table 7. About 18% of the CO_2 molecules were found to be weakly adhered onto the carbon surface as they were easily detached at room temperature. Larger proportion of those physisorbed by van der Waal's force was desorbed at temperature below 200°C. Subsequent ramping released comparatively lesser proportion of CO_2, with an average of 7.5% (between 300 and 400°C). This proportion could be attributed to those previously adsorbed by the coordinate covalent bonding provided by SNFs on the AC surface, whilst the average total of 10.35%, thermally eluted between 500 and 600°C, are ascribed to those held by a much stronger covalent bond with inorganic potassium species (Dantas *et al.*, 2011).

CONCLUSIONS

Some pretreatment methods prior amination were used to improve the CO_2 selective capture of activated carbon,

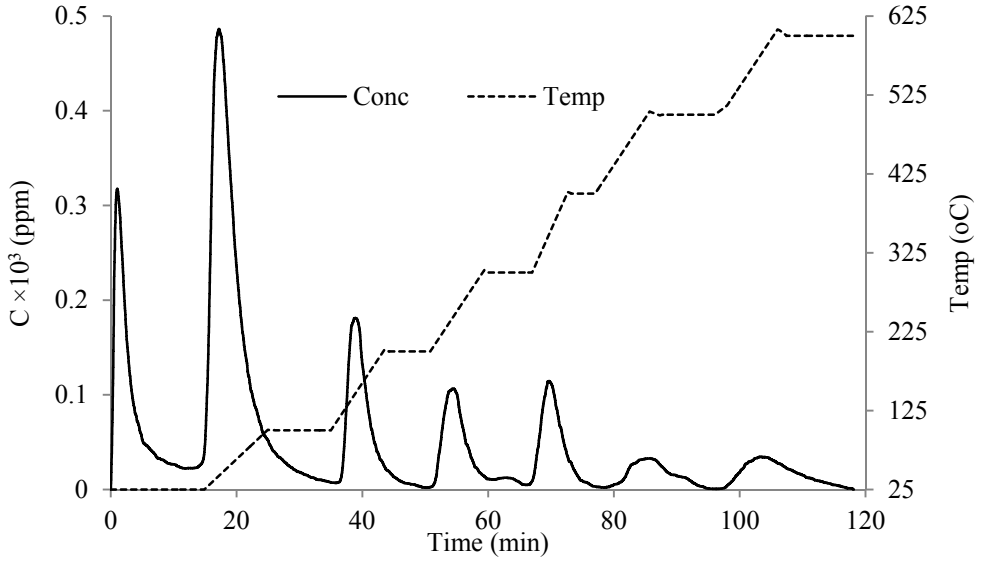

Fig. 9. TPD profiles of 10% CO_2-laden N-4K-N at 600°C.

Table 7. Quantified CO_2 desorbed at each programmed temperature.

Temperature (°C)	Amount of CO_2 desorbed (mmol g^{-1})	% of CO_2 desorbed
25	0.379	17.86
100	0.901	42.82
200	0.261	12.29
300	0.187	8.796
400	0.168	7.880
500	0.096	4.533
600	0.124	5.823

and the adsorption properties were investigated. CO_2 adsorption measurements showed that wet phase peroxidation with KOH is the most suitable method. The nature and degree of tethered basic surface nitrogen functionalities were found to be responsible for CO_2 selective capture while well-developed microporosity as the driving force for pure CO_2 capacity adsorption. Adsorption properties were studied in details. By the conformity of all test samples with Freundlich isotherm, it was conceded that CO_2 molecules bind onto the heterogeneous surface of activated carbon in a monolayer pattern. Also, Redlich-Peterson was the three-parameter model that provided the best fit for expressing the experimental data while Sips model showed a comparatively good fit as well. In general, three-parameter isotherms are more suitable than those of two due to the complex chemical nature of the substrate surfaces. Also, the lowest degree of freedom (highest precision) of error estimation attributed to Chi-square analysis made it the most reliable and efficient of the four error functions used. It was also observed that standard entropy is the major thermodynamic parameter that determines the adsorption process. This was in agreement with the kinetic study, from which CO_2 binding on activated carbon was deduced to follow pseudo-second order and intraparticle diffusion. It indicates the insignificance of the reduction in pure CO_2 capture capacity despite the significant increase in selective adsorption as surface coating was concentrated, accompanied by depreciation in textural properties. The temperature-programmed desorption study finally confirmed the relevance of highly basified activated carbon surface in improving selective adsorptions as more CO_2 molecules were adhered by the various impregnated basic sites. Consequently, the understanding of the adsorption properties in this work provides useful information for adsorption reactor design and regeneration of spent adsorbents used for flue gas and indoor CO_2 scrubbing.

ACKNOWLEDGEMENT

This research was supported by Basic Science Research program through the National Research Foundation of Korea (NRF) funded by the Ministry of Education, Science and Technology (NRF-2015R1D1A1A01060182).

SUPPLEMENTARY MATERIAL

Supplementary data associated with this article can be found in the online version at http://www.aaqr.org.

REFERENCES

Adelodun, A.A. and Jo, Y.M. (2013). Integrated basic treatment of activated carbon for enhanced CO_2 selectivity. *Appl. Surf. Sci.* 286: 306–313.

Adelodun, A.A., Lim, Y.H. and Jo, Y.M. (2014a). Effect of UV-C on pre-oxidation prior amination for preparation of a selective CO_2 adsorbent. *J. Anal. Appl. Pyrolysis* 105: 191–198.

Adelodun, A.A., Lim, Y.H. and Jo, Y.M. (2014b). Stabilization of potassium-doped activated carbon for enhanced CO_2 selective capture. *J. Anal. Appl. Pyrolysis* 108: 151–159.

Adelodun, A.A., Kim, K.H., Ngila, J.C. and Szulejko, J. (2015). A review on the effect of amination pretreatment for the selective separation of CO_2. *Appl. Energy* 158: 631–642.

Aharoni, C. and Tompkins, F.C. (1970). Kinetics of adsorption and desorption and the elovich equation. *Adv. Catal.* 21: 1–49.

Anirudhan, T.S. and Suchithra, P.S. (2010). Equilibrium, kinetic and thermodynamic modeling for the adsorption of heavy metals onto chemically modifies hydrotalcite. *Indian J. Chem. Technol.* 17: 247–259.

Barrett, E.P., Joyner, L.G. and Halenda, P.P. (1951). The determination of pore volume and area distributions in porous substances I. computations from nitrogen isotherms. *J. Amer. Chem. Soc.* 73: 373–382.

Boulinguiez, B., Le Cloirec, P. and Wolbert, D. (2008). Revisiting the determination of langmuir prameters application to tetrahydrothiophene adsorption onto activated carbon. *Langmuir* 24: 6420–6424.

Brdar, M., Sciban, M., Takaci, A. and Dosenovic, T. (2012). Comparison of two and three parameters adsorption isotherm for Cr(VI) onto Kraft lignin. *Chem. Eng. J.* 183: 108–111.

Cáceres-Jensen, L., Rodríguez-Becerra, J., Parra-Rivero, J., Escudey, M., Barrientosa, L. and Castro-Castillo, V. (2013). Sorption kinetics of diuron on volcanic ash derived soils. *J. Hazard. Mater*. 261: 602–613.

Dabrowski, A. (2001). Adsorption – From theory to practice. *Adv. Colloid Interface Sci*. 93: 135–224.

Dali, A.M., Ibrahem, A.S. and Hadi, A. (2012). General study about activated carbon for adsorption of carbon dioxide. *J. Purity Util. React. Environ.* 1: 236–251.

Dantas, T.L.P., Luna, F.M.T., Silva Jr. I.J., de Azevedo, D.C.S., Grande, C.A., Rodriques, A.E. and Moreira, R.F.M. (2011). Carbon dioxide–nitrogen separation

through adsorption on activated carbon in a fixed bed. *Chem. Eng. J.* 169: 11–19.

Deng, S., Chen, T., Zhao, T., Yao, X., Wang, B., Huang, J., Wang, Y. and Yu, G. (2016). Role of micropores and nitrogen-containing groups in CO_2 adsorption on indole-3-butyric acid potassium derived carbons. *Chem. Eng. J.* 286: 98–105.

Diez, N., Alvarez, P., Granda, M., Blanco, C., Santamaria, R. and Menendaz, R. (2015). CO_2 adsorption capacity and kinetics in nitrogen-enriched activated carbon fibers prepared by different methods. *Chem. Eng. J.* 281: 704–712.

Erdem, M., Ucar, S., Karagoz, S. and Tay, T. (2013). Removal of lead (II) ions from aqueous solutions onto activated carbon derived from waste biomass. *Sci. World J.* 2013: 14092.

Faltynowicz, H., Kacz marzyk, J. and Kulazynski, M. (2015). Preparation and characterization of activated carbons from biomass material – giant knotweed (Reynoutria sachalinensis). *Open Chem*. 13: 1150–1156.

Foo, K.Y. and Hamed, B.H. (2010). Insights into the modeling of adsorption isotherm systems. *Chem. Eng. J.* 150: 2–10.

Freundlich, M.F. (1906). Over the adsorption in solution. *J. Phys. Chem*. 57: 355–471.

Gao, J., Yin, J., Zhu, F., Chen, X., Tong, M., Kang, W., Zhou, Y. and Lu, J. (2016). Experimental study of a hybrid solvent MEA-Methanol for post-combustion CO_2 absorption in an absorber packed with three different packing: Sulzer BX500, Mellapale Y500, Pall rings 16 × 16. *Sep. Purif. Technol.* 163: 23–29.

GCCS (2012). Global Climate Change and Society (GCCS) Institute- CO_2 Capture Technologies; Technology Options for CO_2 Capture, January Publication Report.

Goel, C., Bhunia, H. and Bajpai, P.K. (2016). Novel nitrogen enriched porous carbon adsorbents for CO_2 capture: Breakthrough adsorption study. *J. Environ. Chem. Eng*. 4: 346–356.

Gray, M.L., Soong, Y., Champagne, K.J., Baltrus, J., Stevens Jr, R.W., Toochinda, P. and Chuang, S.S.C. (2004). CO_2 Capture by amine-enriched fly ash carbon sorbents. *Sep. Purif. Technol.* 35: 31–36.

Guo, B., Chang, L. and Xie, K. (2006). Adsorption of carbon dioxide on activated carbon. *J. Nat. Gas Chem.* 15: 223–229.

Hamdaoui, O. and Naffrechoux, E., (2007). Modeling of adsorption isotherms of phenol and chlorophenols onto granular activated carbon: Part I. Two-parameter models and equations allowing determination of thermodynamic parameters. *J. Hazard. Mater*. 147: 381–394.

Ho, Y.S. and Ofomaja, A.E. (2006). Pseudo-second-order model for lead ion sorption from aqueous solutions onto palm kernel fiber. *J. Hazard. Mater*. 129: 137–142.

IPCC (2005). *IPCC Special Report on Carbon dioxide Capture and Storage*, Cambridge University Press, Cambridge, UK.

Khalil, S.H., Aroua, M.K. and Wan Daud, W.M.A. (2012). Study on the improvement of the capacity of amine-impregnated commercial activated carbon beds for CO_2 adsorbing. *Chem. Eng. J.* 183: 15–30.

Kongnoo, A., Intharapat, P., Worathanakul, P. and Phalakornkule, C. (2016). Diethanolamine impregnated palm shell activated carbon for CO_2 adsorption at elevated temperatures. *J. Environ. Chem. Eng*. 4: 973–983.

Kulshreshtha, P., Khare, M. and Seetharaman, P. (2008). Indoor air quality assessment in and around urban slums of Delhi City, India. *India Indoor Air* 18: 488–498.

Kumar, K.V. (2006). Comparative analysis of linear and non-linear method of estimating the sorption isotherm parameters for malachite green onto activated carbon. *J. Hazard. Mater.* 136: 197–202.

Kumar, K.V. (2007). Optimum sorption isotherm by linear and non-linear methods for malachite green onto lemon peel. *Dyes Pigm.* 74: 595–597.

Langmuir, I. (1916). The constitution and fundamental properties of solids and liquids. *J. Amer. Chem. Soc.* 38: 2221–2295.

Li, J. and Hitch, M. (2016). Carbon dioxide adsorption isotherm study on mine waste for integrated CO_2 capture and sequestration. *Powder Technol.* 291: 408–413.

Lim, Y.H., Adelodun, A.A. and Jo, Y.M. (2014). adsorption of low-level CO_2 using activated carbon pellet with glycine metal salt impregnation. *J. Korean Soc. Atmos. Environ.* 30: 68–76.

Ma, X., Li, L., Wang, S., Lu, M., Li, H., Ma, W. and Keener. T.C. (2016). Ammonia-treated porous carbon derived from ZIF-8 for enhanced CO_2 adsorption. *Appl. Surf. Sci.* 369: 390–397.

Michael, G.A. and William, M.D. (2000). Indoor Carbon Dioxide Concentrations and SBS in Office Workers. Proceedings of Healthy Buildings, pp. 133–138.

Mikhail, R.S., Brunauer, S. and Bodor, E.E. (1968). Investigations of a complete pore structure analysis I. analysis of microstructure. *J. Colloid Interface Sci.* 26: 45–49.

Mittal, A., Kurup, L. and Mittal, J. (2007). Freundlich and langmuir adsorption isotherms and kinetics for the remocal of tartrazine from aqueous solutions using hen feathers. *J. Hazard. Mater.* 146: 243–248.

Olajire, A.A. (2010). CO_2 capture and separation technologies for end-of-pipe applications – A review. *Energy* 35: 2610–2628.

Ozacar, M. and Sengil, I.A. (2005). A kinetic study of metal complex dye sorption onto pine sawdust. *Process Biochem.* 40: 565–572.

Pevida, C., Plaza, M.G., Arias, B., Fermoso, J., Rubiera, F. and Pis, J.J. (2008). Surface modification of activated carbon for CO_2 capture. *Appl. Surf. Sci.* 254: 7165–7172.

Plaza, M.G., Pevida, C., Arias, B., Fermoso, J., Casal, M.D., Martin, C.F., Rubiera, F. and Pis, J.J. (2009b). Development of low-cost biomass-based adsorbents for postcombustion CO_2 capture. *Fuel* 88: 2442–2447.

Plaza, M.G., Pevida, C., Arias, B., Fermoso, J., Rubiera, F. and Pis, J.J. (2009a). A comparison of two methods for producing CO_2 captures adsorbents. *Energy Procedia* 1: 1107–1113.

Qui, H., Lu, L.V., Pan, B.C., Zhang, Q.J., Zhang, W.M. andZhang, Q.X. (2009). Critical review in adsorption

kinetic models. *J. Zhejiang Univ. Sci. A* 10: 716–724.

Redlich, O. and Peterson, D.L. (1959). A useful adsorption isotherm. *J. Phys. Chem*. 63: 1024–1026.

Schrag, D.P. (2007). Preparing to capture carbon. *Science* 315: 812–813.

Shafeeyan, M.S., Wan Daud, W. A., Shamiri, A. and Aghamohammadi, N. (2015). Adsorption equilibrium of carbon dioxide on ammodia-modified activated carbon. *Chem. Eng. Res. Des.* 104:42–52.

Shafeeyan, M.S., Wan Daud, W.M.A., Houshmand, A. and Shamiri, A. (2010). A review on surface modification of activated carbon adsorption. *J. Anal. Appl. Pyrolysis* 89: 143–151.

Shah, K.J. and Imae, T. (2016). Analytical investigation of specific adsorption kinetics of CO_2 gas on dendrimer loaded in organoclays. *Chem. Eng. J*. 283: 1366–1373.

Sips, R. (1948). Combined form of langmuir and freundlich equations. *J. Phys. Chem*. 16: 490–495.

Song, G., Zhu, X.Z., Liao, Q., Ding, Y.D. and Chen, L. (2016). An investigation of CO_2 adsorption kinetics on porous magnesium oxide. *Chem. Eng. J*. 283: 175–183.

Subramanyan, B. and Das, A. (2009). Linearized and non-linearized isotherm models comparative study on adsorption of aqueous phenol solution in soil. *Int. J. Environ. Sci. Technol*. 6: 633–640.

Temkin, M.I. and Pyzhev, V. (1940). Kinetics of ammonia synthesis on promoted iron catalyst. *Acta Phys. Chem* USSR 12: 327–356.

Toth, J. (1971). State equations of the solid gas interface layer. *Acta Chem. Acad. Hung*. 69: 311–317.

Valderrama, C., Cortina, J.L., Farran, A., Gamisans, X. and Lao, C. (2007). Kinetics of sorption of polyaromatic hydrocarbons onto granular activated carbon and Macronet hyper-crosslinked polymers (MN200). *J. Colloid Interface Sci.* 310: 35–46.

Xiao, G., Singh, R., Chaffee, A. smf Webley, P. (2011). Advanced adsorbents based on MgO and K_2CO_3 for capture of CO_2 at elevated temperatures. *Int. J. Greenhouse Gas Control* 5: 634–639.

Yousef, R.I., El-Eswed, B. and Al-Muhtaseb, A.H. (2011). Adsorption characteristics of natural zeolites as solid adsorbents for phenol removal from aqueous solutions: Kinetics, mechanism, and thermodynamics studies. *Chem. Eng. J.* 171: 1143–1149.

Yu, C.H., Huang, C.H. and Tan, C.S. (2012). A review of CO_2 capture by absorption and adsorption. *Aerosol Air Qual. Res.* 12: 745–769.

Yu, Y., Zhang, T., Wu, X., Mu, D., Zhang, Z. and Wang, G.G. (2015). Mass and heat transfer characteristic in MEA absorption of CO_2 improved by meso-scale method. *Int. J. Greenhouse Gas Control* 47:310–321.

Zhang, X.Q., Li, W.C. and Lu, A.H. (2015). Designed porous carbon materials for efficient CO_2 adsorption and separation. *New Carbon Mater.* 30: 481–501.

Zhou, Z., Mei, L., Ma, C., Xu, F., Xiao, J., Xia, Q. and Li, Z. (2016). a novel bimetallic MIL-101 (Cr, Mg) with high CO_2 adsorption capacity and CO_2/N_2 selectivity. *Chem. Eng. Sci.* 147: 109–117.

Received for review, January 24, 2016
Revised, June 27, 2016
Accepted, July 10, 2016